ISSN 1070-4272, Russian Journal of Applied Chemistry, 2019, Vol. 92, No. 8, pp. 1170−1178. © Pleiades Publishing, Ltd., 2019.
Russian Text © The Author(s), 2019, published in Zhurnal Prikladnoi Khimii, 2019, Vol. 92, No. 8, pp. 1079−1088.

ORGANIC SYNTHESIS AND INDUSTRIAL ORGANIC CHEMISTRY

Ruthenium Catalysts on ZSM-5/MCM-41 Micro-Mesoporous Support for Hydrodeoxygenation of Guaiacol in the Presence of Water

E. A. Roldugina[a,*], A. P. Glotov[b], A. L. Isakov[a], A. L. Maksimov[a,c], V. A. Vinokurov[b], and E. A. Karakhanov[a]

[a] *Chemistry Department, Moscow State University, Moscow, 119991 Russia*
[b] *Gubkin University, National University of Oil and Gas, Moscow, 119991 Russia*
[c] *Topchiev Institute of Petrochemical Synthesis, Moscow, 119991 Russia*
**e-mail: rolduginakate@mail.ru*

Received May 25, 2019; revised June 17, 2019; accepted June 17, 2019

Abstract—A ruthenium-containing catalyst on ZSM-5/MCM-41 micro-mesoporous aluminosilicate support was synthesized. The micro-mesoporous support and supported catalyst were characterized by low-temperature nitrogen desorption/adsorption, temperature-programmed ammonia desorption, transmission electron microscopy, X-ray photoelectron spectroscopy, temperature-programmed reduction with hydrogen, and energy-dispersive X-ray fluorescence analysis. Ru/ZSM-5/MCM-41 has high specific surface area (392 $m^2\ g^{-1}$) and high acidity (1087 μmol g^{-1}); the mean ruthenium particle size is 1.7 nm. The catalyst was studied in hydrodeoxygenation of a modelbio-oil compound, guaiacol, in the presence of water at a hydrogen pressure of 5 MPa and temperatures in the interval 130–290°C. The catalyst obtained exhibits high activity in guaiacol hydrodeoxygenation: The conversion was 90%, and the selectivity with respect to cycloalkanes was 64% in 3-h reaction performed at a hydrogen pressure of 5 MPa and a temperature of 230°C.

Keywords: nanoparticles, guaiacol, micro-mesoporous materials, hydrodeoxygenation, ruthenium

DOI: 10.1134/S1070427219080172

Lignocellulosic biomass, a wood waste from nonfood industry, is a promising biological raw material, because its processing supports the zero balance of CO_2 in the atmosphere and allows production of biofuel with the characteristics similar to those of the existing motor fuels [1]. The biomass processing by the fast pyrolysis technology yields so-calledbio-oil differing from other biofuels in the convenience of storage and transportation and in the complexity of the composition, which allows using it not only as a transport fuel but also as feedstock for fine chemical synthesis.bio-oil contains hundreds of organic compounds formed by thermal degradation of cellulose and lignin and belonging to different classes, such as low-molecular-weight alcohols, acids, ethers, esters, aldehydes, ketones, furans, and phenols of various structures. Complex chemical composition and high content of water formed by biomass polymer degradation and of oxygen are responsible for high polarity, high acidity, and thermal instability ofbio-oil [1]. The removal of oxygen and water frombio-oil and its joint processing with hydrocarbon petroleum products on traditional oil-refining equipment require an additional stage of improving thebio-oil quality. A promising technology for processing biological raw materials is catalytic hydrotreating (hydrodeoxygenation, HDO), in whichbio-oil components undergo such catalytic transformations as cracking, decarbonylation, decarboxylation, deoxygenation, and hydrogenation [2].

One of the factors ensuring the hydrodeoxygenation efficiency is the development of stable and ac-

tive catalysts. The traditional HDO catalyst contains an active phase, metal particles immobilized on a solid support. Three types of catalysts forbio-oil hydrodeoxygenation are known: traditional sulfidized hydrotreating catalysts $NiMo/Al_2O_3$ and $CoMo/Al_2O_3$ [3]; heterogeneous catalysts based on transition metals (Ni [4], Mo [5], W [6], Fe [7] Cu [8], etc.); and catalysts based on noble metals (Rh, Ru, Pt, and Pd [9, 10]). Catalysts based on noble metals, in particular, Ru-containing catalysts exhibiting high activity in processes performed in the presence of water [11–14] formed in large amounts inbio-oil HDO, are of interest in this respect. The support is an important component of hydrodeoxygenation catalysts; its textural and acid characteristics significantly influence the reaction product distribution and the deoxygenation efficiency. Initially classical γ-Al_2O_3 was used as a catalyst support inbio-oil processing; however, in the presence of water γ-Al_2O_3 transforms into boehmite AlO(OH), which can cause blocking and deactivation of the catalyst active sites [15]. The following supports are used as alternatives to γ-Al_2O_3: zeolites [16], carbon supports [9], SiO_2 [9], ZrO_2 [10], CeO_2, TiO_2 [17, 18], and their mixtures [9, 19]. Mesoporous inorganic supports are of particular interest for hydrodeoxygenation processes [11, 20–26]. It is assumed that their developed structure reduces the diffusion hindrance and favors enhancement of the catalytic activity, and the optimum acidity level ensures efficient deoxygenation [27–29].

One of model compounds frequently used for studying the relationships ofbio-oil hydrodeoxygenation is guaiacol, because it contains both hydroxyl ($C_{sp2}OH$), and methoxy ($C_{sp2}OCH_3$) fragments as the most typical fragments of oxygen-containing phenolic components ofbio-oil [1]. Because it is known thatbio-oil contains a large amount of water released from plant cell walls in the course of biomass pyrolysis and formed by hydrotreating of thebio-oil itself, it is necessary to evaluate the effect of water on the catalytic system. Therefore, in studying guaiacol HDO, we chose water as the second component of the reaction mixture.

Thus, our goal was to evaluate the activity of Ru-containing catalysts supported on ZSM-5/MCM-41 micro-mesoporous material in hydrodeoxygenation of a model compound ofbio-oil, guaiacol, in the presence of water.

EXPERIMENTAL

Synthesis of ZSM-5/MCM-41 micro-mesoporous material. ZSM-5/MCM-41 (Si/Al = 16) was prepared by the procedure similar to that described in [30]. The following chemicals were used: cetyltrimethylammonium bromide (CTAB, Sigma–Aldrich, 98%), sodium aluminate (Sigma–Aldrich), pyrogenic silica (Sigma–Aldrich, 99.99%), tetrapropylammonium hydroxide (TPAOH, Sigma–Aldrich, 1 M aqueous solution), sodium hydroxide (Irea 2000, chemically pure grade), and distilled water. The gel containing templates of ZSM-5 and mesoporous material had the following molar composition: $3.1Na_2O : 31SiO_2 : Al_2O_3 : 1.9CTAB : 0.23TPAOH : 854H_2O$.

Synthesis of Ru/ZSM-5/MCM-41 catalyst. A typical procedure for preparing Ru/ZSM-5/MCM-41 includes impregnation of the support with an aqueous solution of ruthenium chloride, taken in an amount corresponding to the moisture capacity, followed by solvent removal on a water bath in an air stream. To this end, a calculated amount of the support was added to a solution of the metal salt at 25°C. After adding the impregnating solution to the support, the liquid layer over it did not exceed 2 mm. The mixture was stirred for 10-min periods with 10-min breaks (total time 2 h) and left overnight for impregnation. After that, the sample was dried in an air stream at 60°C for 6 h, at 100°C for 3 h, and finally at 250°C for 3 h and was reduced in a hydrogen stream at 400°C for 3 h. Ruthenium(III) chloride (Aurat, ruthenium weight fraction no less than 46.5%) was used as a metal source. When preparing the metal salt solution, the $RuCl_3$ amount was calculated so as to ensure 1 wt % ruthenium content of the catalyst.

Devices and methods. The nitrogen adsorption/desorption isotherms were recorded at 77 K with a Gemini VII 2390 device. Prior to measurements, the samples were degassed at 350°C for 6 h. The specific surface area was calculated by the BET method using the adsorption data in the relative pressure range p/p_0 = 0.04–0.20. The pore volume and pore-size distribution were determined from the adsorption branch of the isotherms using the Barrett–Joyner–Halenda model. The micropore volume was determined using the Horvath–Kawasoe model. The specific pore volume was determined from the amount of adsorbed nitrogen at the relative pressure $p/p_0 = 0.99$.

The acidity of the catalyst sample was determined by temperature-programmed ammonia desorption (TPD-

NH_3) with a Micromeritics AutoChem HP chemisorption analyzer. The sample was finely divided, and the 1–2-mm fraction was taken, placed in a reactor, and kept in a helium flow at 400°C for 30 min, after which the temperature was decreased to 100°C, and the sample was saturated with ammonia for 30 min. Physically adsorbed ammonia was removed in a helium flow until the baseline drift ceased. Then, the temperature was raised to 750°C at a rate of 20 deg min^{-1}. The amount of ammonia desorbed in the course of ammonia TPD was calculated using the AutoChem HP V2.04 program.

A transmission electron microscopic (TEM) study of the catalyst was performed with a Jeol JEM-2100 device (magnification from 50 to 1 500 000, image resolution 0.19 nm at 200 kV).

The ruthenium content was determined by energy-dispersive X-ray fluorescence (EDX) analysis with a Thermo Fisher Scientific ARLQuant'X analyzer in a vacuum. The results were processed using the UniQuant method without references. The samples were prepared as follows: Powdered samples were pressed in pellets on a boric acid support and covered with a Lavsan [material based on poly(ethylene terephthalate)] film, which was pressed to the cell with a special ring.

X-ray photoelectron spectroscopic (XPS) studies were performed with a Kratos Axis Ultra DLD device using AlK_α excitation X-ray radiation (1486.6 eV). The photoelectron peaks were calibrated using the C1*s* line (binding energy 284.8 eV). The transmission energy of the energy analyzer was 160 eV for the total spectrum and 40 eV for separate lines.

Temperature-programmed reduction with hydrogen (TPR-H_2) was performed with a Micromeritics AutoChem HP2950 chemisorption analyzer. Prior to the experiments, the sample was calcined in a muffle furnace in an air stream at 550°C for 4 h to convert the ruthenium to the oxide form. The test sample (~0.1 g) was placed in a quartz reactor and kept for 1 h in an argon flow at 400°C. After that, the temperature was decreased to 60°C, the flow rate of the argon–hydrogen mixture (8 vol % H_2) of 30 mL min^{-1} was set, and the temperature was raised to 400°C at a rate of 10 deg min^{-1}.

Procedure of catalytic experiments. The catalytic experiments on HDO of guaiacol at elevated hydrogen pressure were performed with vigorous stirring in a 10-mL steel autoclave equipped with a magnetic stirrer. The autoclave was charged with the calculated amount of the catalyst (25 mg) and a model mixture consisting of 0.25 g of guaiacol (Sigma–Aldrich, ≥98%) and 0.25 g of water. The autoclave was sealed and filled with hydrogen to a pressure of 5 MPa. The reaction was performed in the temperature interval 130–290°C for 3 h; the temperature was monitored with a thermocouple. After the reaction completion, the autoclave was cooled below the room temperature and opened. The catalyst was separated from the solution by centrifugation. For complete dissolution of organic compounds and homogenization of the reaction mixture, isopropanol (Irea 2000, analytically pure grade) was added to the sample prior to chromatographic analysis. The hydrogenation products were analyzed with a Kristallyuks 4000 M chromatograph equipped with a flame ionization detector and a Petrocol® DH 50.2 capillary column (50 m × 0.25 mm, stationary phase polydimethylsiloxane). The carrier gas was helium (flow split ratio 1 : 90). The liquid products were additionally analyzed by gas chromatography–mass spectrometry with a Finnigan MAT 95 XL device. Its chromatograph was equipped with a Varian VF-5MS capillary column (30 m × 0.25 mm × 0.25 μm); the carrier gas was helium (1.5 cm^3 min^{-1}).

RESULTS AND DISCUSSION

The textural characteristics of the Ru/ZSM-5/MCM-41 catalyst were determined by low-temperature nitrogen adsorption–desorption. Ru/ZSM-5/MCM-41 is characterized by the adsorption–desorption isotherm of type IV with a hysteresis loop confirming the mesoporous structure (Fig. 1) [30, 31].

The catalyst obtained has high specific surface area and high specific pore volume: S_{BET} = 392 m^2 g^{-1}, V_{pore} = 0.41 cm^3 g^{-1} (Table 1). After impregnation of the micro-mesoporous support with the ruthenium salt, the specific surface area decreased only slightly. Thus, application of 1 wt % metal does not significantly affect the texture characteristics of the catalyst.

The Ru/ZSM-5/MCM-41 catalyst was studied by TPD-NH_3 (Table 2). Depending on the temperature ranges of the ammonia desorption, the acid sites can be subdivided into weak (T < 300°C), medium-strength (T = 300–500°C), and strong (T > 500°C). The Ru/ZSM-5/MCM-41 sample exhibits high acidity (1087 μmol g^{-1}) and contains mainly medium-strength acid sites (841 μmol g^{-1}) with small amounts of weak (90 μmol g^{-1}) and strong (157 μmol g^{-1}) acid sites.

Table 1. Textural characteristics of micro-mesoporous aluminosilicate and catalyst based on it

Sample	BET specific surface area, $m^2\ g^{-1}$	Micropore surface area, $m^2\ g^{-1}$	Pore volume, $cm^3\ g^{-1}$	Pore diameter, Å	Micropore volume, $cm^3\ g^{-1}$	Fraction of micropores (S_{micro}/S_{BET})
ZSM-5/MCM-41	425	77	0.43	39	0.02	0.18
Ru/ZSM-5/MCM-41	392	74	0.41	42	0.06	0.19

Table 2. TPD-NH_3 data for Ru/ZSM-5/MCM-41

Sample	Acid sites, μmol g^{-1}			Total amount of acid sites, μmol g^{-1}
	weak	medium	strong	
Ru/ZSM-5/MCM-41	90	841	157	1087

The thermal desorption curve has a pronounced maximum at approximately 320°C, corresponding to medium-strength acid sites, and weaker peaks at approximately 160 and 550°C, corresponding to weak and strong acid sites (Fig. 2).

TEM examination confirms that the ZSM-5/MCM-41 support is a crystalline mesophase material with lamellar structure [30]. The secondary mesoporous structure is formed via formation of slitlike voids, caused by deformation of the hexagonal framework of MCM-41 in the course of the zeolite crystallization. Ordered pores with a size of approximately 30–40 Å are seen in the electron micrographs. The porous structure of ZSM-5 zeolite can be clearly observed at high resolution of the images (Fig. 3b). According to the TEM data, ruthenium particles are uniformly distributed over the support surface. Their mean size is approximately 1.7 nm; coarser particles (up to 6 nm) are present in a small amount (Figs. 3c. 3d). The appearance of coarser particles may be due to agglomeration of nanosized particles in the course of the catalyst reduction in a hydrogen stream at elevated temperature [32].

The curve of the temperature-programmed reduction of Ru/ZSM-5/MCM-41 sample with hydrogen has two peaks at 106 and 253°C [22], with the first peak having a shoulder at 130–160°C (Fig. 4). The first maximum corresponds to the reduction of RuO_2 on the external surface of ZSM-5/MCM-41 [33, 34]. The broad shoulder can be attributed to the reduction of ruthenium oxides and oxychlorides tightly bound to the surface of the micro-mesoporous support; it requires higher temperatures [34]. The maximum at 253°C belongs

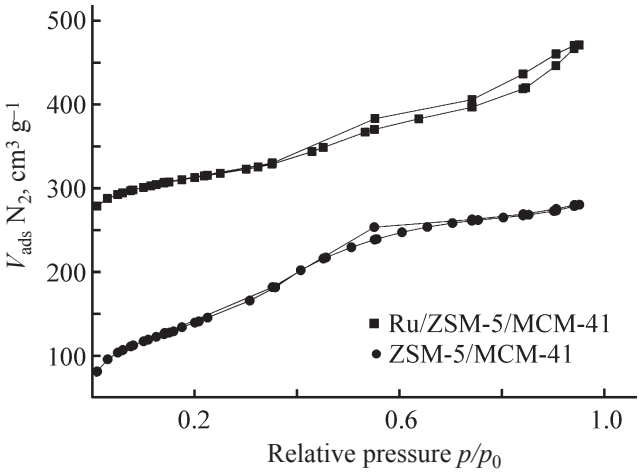

Fig. 1. Nitrogen adsorption/desorption isotherms for Ru/ZSM-5/MCM-41 and ZSM-5/MCM-41.

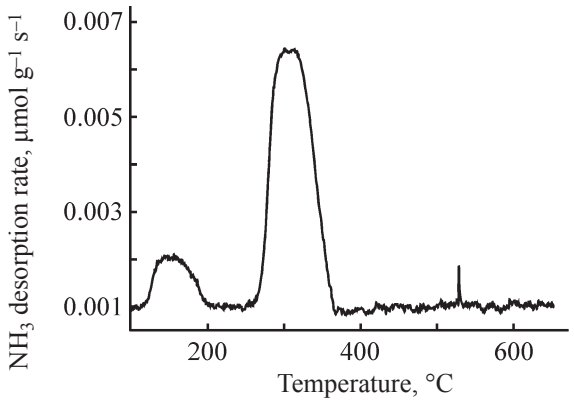

Fig. 2. Temperature-programmed ammonia desorption spectrum of Ru/ZSM-5/MCM-41.

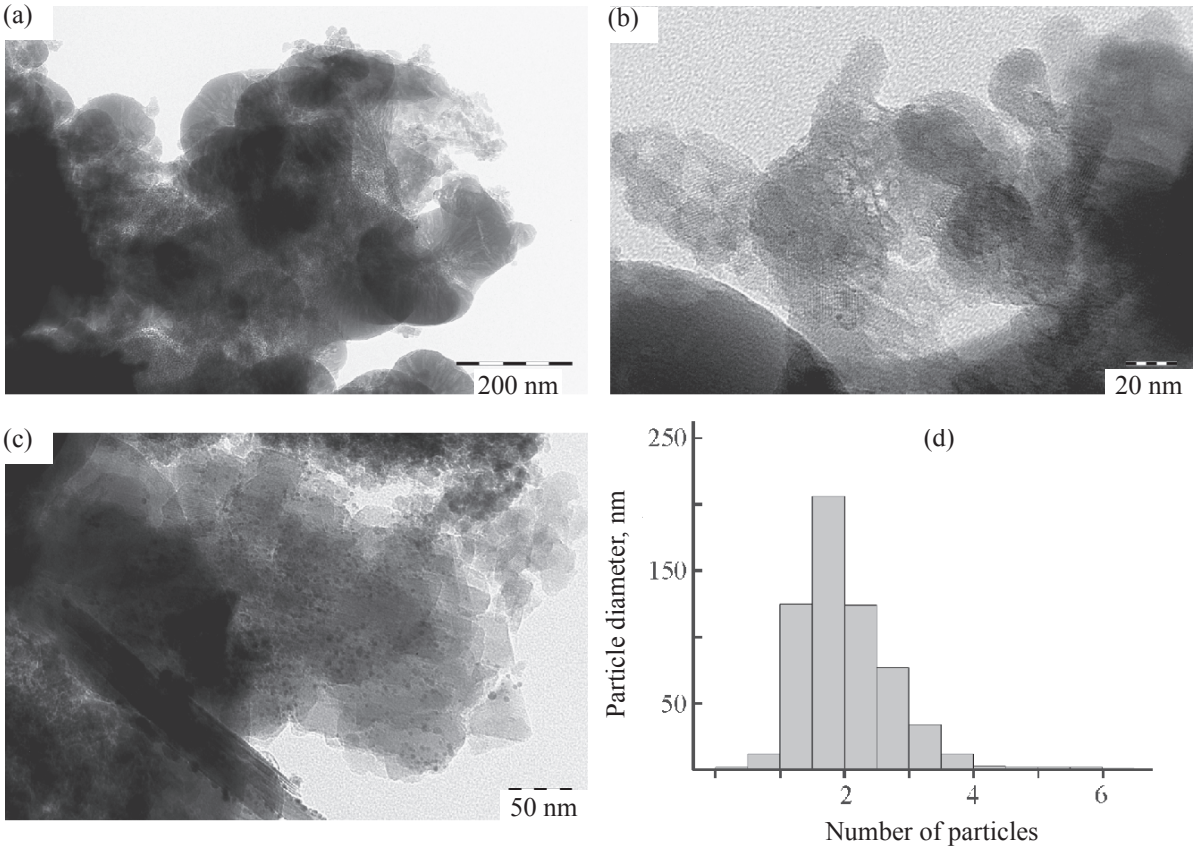

Fig. 3. TEM images of (a, b) ZSM-5/MCM-41 and (c) Ru/ZSM-5/MCM-41 and (d) ruthenium particle size distribution.

to the reduction of difficultly accessible ruthenium in narrow pores of ZSM-5/MCM-41 [35].

According to the TPR-H_2 data (Table 3), the ruthenium content of Ru/ZSM-5/MCM-41 is 1.0 wt %, which is confirmed by elemental analysis. The most pronounced hydrogen uptake is observed at 106°C (0.194 mmol g^{-1}), suggesting the formation of ruthenium nanoparticles mainly on the surface of the micro-mesoporous material.

Figure 5 shows the high-resolution Ru3*d* fragment of the XPS spectrum of Ru/ZSM-5/MCM-41. Because of the overlap of the C1*s* (285 eV) and Ru3$d_{3/2}$ lines, only the Ru3$d_{5/2}$ component (280.1 eV) could be identified reliably. However, the spectrum deconvolution revealed the presence of two states of Ru, Ru3$d_{5/2}$ and Ru3$d_{3/2}$, with the binding energies of 279.9 and 283.8 eV, which corresponds to ruthenium metal [32, 36]. Also, there

Table 3. TPR-H_2 data for Ru/ZSM-5/MCM-41

Peak temperatures in the reduction curves, °C	106/253
Amount of adsorbed H_2, μmol g_{cat}^{-1}	0.194/0.01
Ruthenium content,[a] wt %	1.0

[a] Calculated assuming complete reduction of RuO_2.

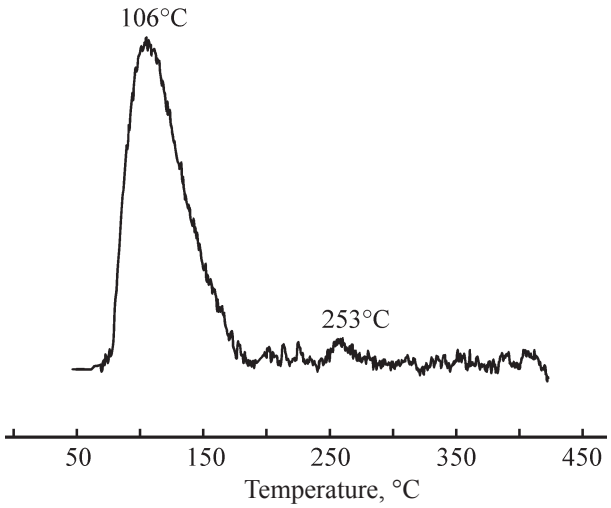

Fig. 4. Curve of temperature-programmed reduction of Ru/ZSM-5/MCM-41 with hydrogen.

are maxima in the spectra at the energies of 280.8 and 285.2 eV, corresponding to ruthenium in the oxidized state [36].

The catalytic activity of the Ru/ZSM-5/MCM-41 sample obtained was evaluated in hydrodeoxygenation of a modelbio-oil compound, guaiacol, at 5 MPa of H_2 in the temperature interval 130–290°C for 3 h. The guaiacol/water weight ratio equal to 1 was chosen to make the model mixture composition similar to that of the realbio-oil, in which the water content can vary in the interval 15–40 wt % depending on the initial biomass composition and pyrolysis conditions [1]. It should be noted that, in HDO experiments, an aqueous solution containing no more than 8 wt % substrate is used as a model mixture [9, 16]. This study was aimed at evaluating the behavior of the catalyst in the presence of a large amount of one of phenolicbio-oil components, guaiacol (50% aqueous solution).

We have studied the activity of Ru/ZSM-5/MCM-41 in HDO of guaiacol in the temperature interval 130–290°C. At 130°C, the guaiacol conversion was 45% (Fig. 6); on heating to 150°C, the conversion sharply increased to 98%. In the temperature interval 150–210°C, the conversion was close to 100%. As the reaction temperature was increased further, the guaiacol conversion gradually decreased (to 90% at 230°C). At still higher temperatures, the conversion decreased drastically: to 68% at 250°C, reaching a constant value of ~50% at 270–290°C.

The reaction temperature significantly influences the distribution of guaiacol HDO products (Fig. 7). HDO of guaiacol at 130°C yielded products of direct hydrogenation of the guaiacol aromatic ring: methoxycyclohexanol (selectivity 62%) and hydroxy- and methoxycyclohexanes (O-cyclohexanes, 36%). Cyclohexane, and also phenol and anisole (O-benzenes, ~1%) were detected in trace amounts. The temperature elevation from 150 to 190°C led to a decrease in the methylcyclohexanol content from 55 to 41%, with the amount of O-cyclohexanes remaining on the level of ~40%; the selectivity with respect to cycloalkanes (cyclohexane and trace amounts of methylcyclohexane and methylcyclopentane) gradually increased from 3 to 19%. At 210°C, the reaction mixture composition became considerably more complex. The content of methylcyclohexanol decreased to 24%, and that of hydroxy- and methoxycyclohexanes, to 6% (in total); the selectivity with respect to cycloalkanes sharply

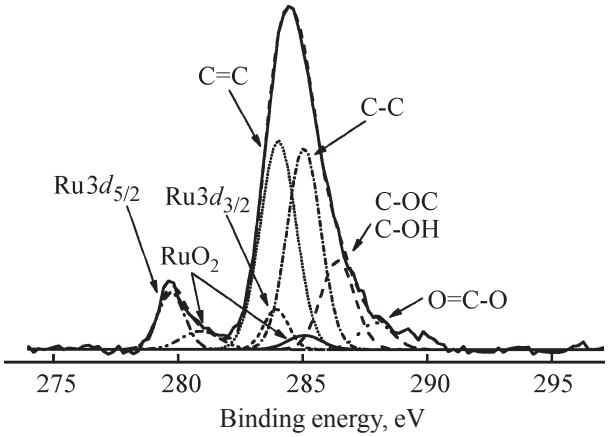

Fig. 5. Ru3*d* X-ray photoelectron spectrum of Ru/ZSM-5/MCM-41.

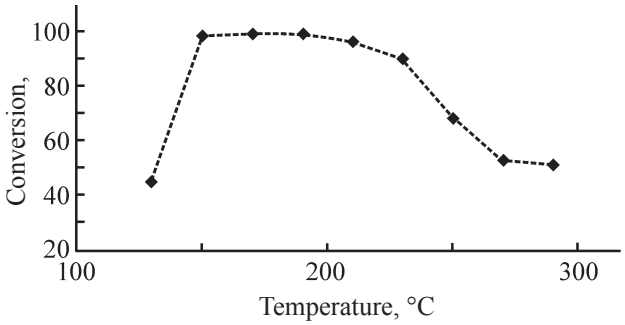

Fig. 6. Guaiacol conversion in the presence of Ru/ZSM-5/MCM-41 catalyst as a function of temperature.

increased, and their content reached 66%. Products of direct deoxygenation of guaiacol, namely, anisole, phenol (O-benzenes, ~1%), benzene (2%), and cyclohexene (2%), were also detected in the reaction products. On further temperature elevation to 250°C, the trend toward active formation of cycloalkanes (with a decrease in the total concentration of O-cyclohexanes and methoxycyclohexanol) and toward a gradual increase in the selectivity with respect to benzenes was preserved. At 250°C, the selectivity with respect to cycloalkanes reached a maximum (78%); the other major products were benzene (10%), phenol, and anisole (O-benzenes, 6%). At this reaction temperature, small amounts of heavier guaiacol HDO products, methyl- and dimethylphenols (polymethylphenols, ≤2%) appeared in the product mixture. Further temperature elevation to 270°C led to a sharp decrease in the concentration of cycloalkanes to 42%; the content of O-cyclohexanes and methoxycyclohexanol did not exceed 2 and 3%, respectively. The fractions of phenol and anisole

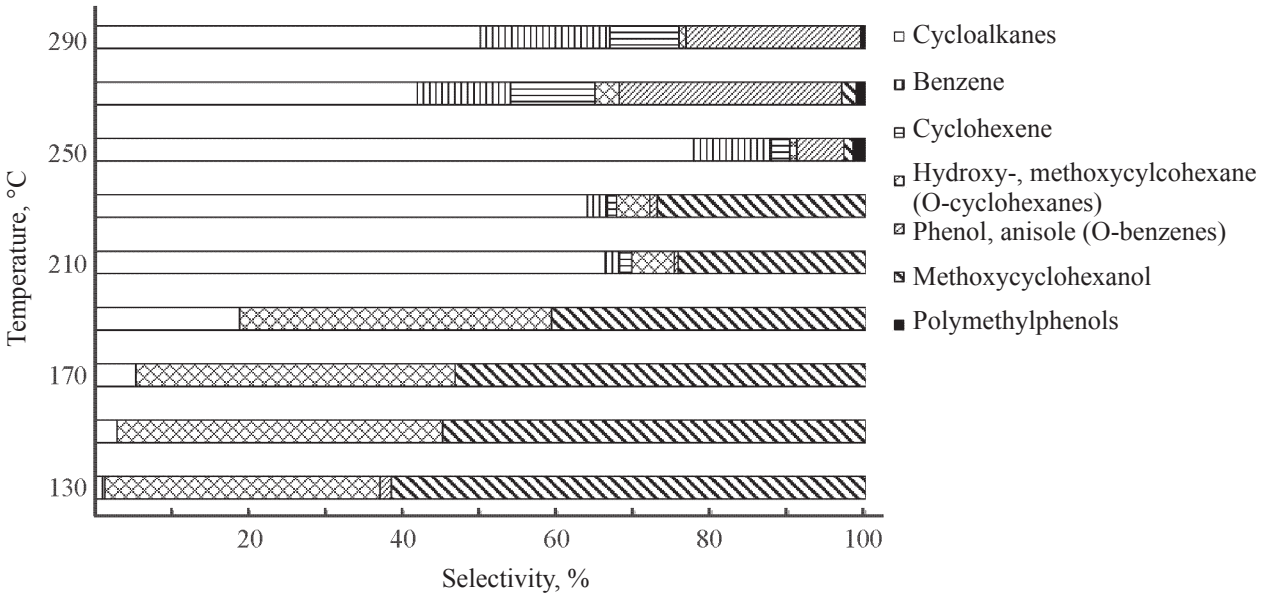

Fig. 7. Product distribution in HDO of guaiacol in the presence of Ru/ZSM-5/MCM-41 catalyst at various temperatures (130–290°C). Cycloalkanes: cyclohexane and trace amounts of methylcyclohexane and methylcyclopentane.

(O-benzenes), benzene, and cyclohexene increased to 29, 12, and 11%, respectively. Elevation of the reaction temperature to 290°C did not lead to significant changes in the reaction product distribution. The selectivity with respect to cycloalkanes slightly increased (to 50%), the content of hydroxy- and methoxycyclohexane (O-cyclohexanes) was 1%, and methoxycyclohexanol was not detected. The selectivity with respect to O-benzenes and cyclohexene slightly decreased: from 29 to 23 and from 11 to 9%, respectively. The selectivity with respect to benzene increased from 12 to 17%. At the reaction temperatures of 270 and 290°C (as at 250°C), polymethylphenols were detected in trace amounts (<2%).

The analysis results suggest that HDO of guaiacol under the conditions of our experiments in the presence of Ru/ZSM-5/MCM-41 occurs along two parallel pathways [37]. At low temperatures (up 210°C), the prevalent process is direct hydrogenation of the aromatic ring of guaiacol, followed by deoxygenation, in accordance with the scheme guaiacol → methoxycyclohexanol → hydroxycyclohexane → methoxycyclohexane → cyclohexane → methylcyclohexane. At 210°C, a side process starts to occur: direct deoxygenation of guaiacol to phenol and anisole and then to benzene, followed by hydrogenation of benzene to cyclohexene and cyclohexane (guaiacol → phenol → anisole → benzene → cyclohexene → cyclohexane). With increasing temperature, the contribution of this pathway increases: At 290°C, the selectivity with respect to benzene is 19%. In the temperature interval 210–250°C, the reaction rates for the first pathway increase, which is manifested in a sharp increase in the selectivity with respect to cycloalkanes (to 78% at 250°C) with a decrease in the selectivity with respect to hydroxy- and methoxycyclohexanes and to methoxycyclohexanol to 2% (in total). At reaction temperatures higher than 250°C, cycloalkanes were detected in the reaction products (>40%), with O-cyclohexanes and methoxycyclohexanol virtually disappearing. As compared to lower temperatures, the products of the reaction at 270°C contained considerably more phenol and anisole (O-benzenes, 6% at 250°C and 29% at 270°C). The other major intermediates were benzene and cyclohexene. Such product distribution indicates that, when HDO is performed at elevated temperatures (>250°C), the second pathway, direct guaiacol deoxygenation to benzene, followed by its hydrogenation, prevails.

The occurrence of HDO along two pathways is possible owing to bifunctional properties of the Ru/ZSM-5/MCM-41 catalyst: Hydrogenation of the aromatic ring occurs on metallic active sites of the catalyst [9, 16], and deoxygenation, on acid sites of the micro-mesoporous support [32, 37]. For the efficient deoxygenation, the catalyst should have a large number of acid sites ac-

tive in the given temperature interval; however, strong acid sites favor the formation of polymethylation by-products, which act as coke precursors and decrease the catalyst activity [32]. It should be noted that, in HDO of guaiacol in the presence of Ru/ZSM-5/MCM-41 catalyst exhibiting high acidity (1087 μmol g^{-1}) but containing only a small amount of strong acid sites (Fig. 2), the selectivity with respect to polymethylphenols does not exceed 2% even at elevated temperatures (>250°C). The developed hierarchic structure of the support, ZSM-5/MCM-41, ensures the maximal access of reagents to active sites of the catalyst, which is manifested in high parameters of guaiacol conversion at moderate reaction temperatures. However, at temperatures higher than 250°C, the guaiacol conversion sharply decreases from >90 to 50%. This may be associated with the catalyst deactivation at elevated temperatures, caused by the formation of intermediate products [anisole, phenol (O-benzenes), polymethylphenols], which can be adsorbed on active sites of the catalyst more strongly than guaiacol [38, 39].

CONCLUSIONS

The hydrogenation of guaiacol in the presence of water at the water/guaiacol weight ratio of 1 on a ruthenium catalyst on ZSM-5/MCM-41 micro-mesoporous support was studied. The reaction can occur along two pathways: hydrogenation of the guaiacol aromatic ring, followed by deoxygenation of oxygen-containing groups, or direct deoxygenation of guaiacol with the formation of benzene, followed by its hydrogenation to cyclohexane. The temperature strongly influences the reaction mechanism: The hydrogenation/deoxygenation with the highly selective formation of cyclohexane prevails at temperatures of up to 250°C, whereas at higher temperatures the direct deoxygenation with the formation of benzene and then cyclohexane occurs more actively. In the temperature interval 150–230°C, the guaiacol conversion reaches >90%, but at further temperature elevation it decreases to 50%.

FUNDING

The study was financially supported by the Ministry of Science and Higher Education of the Russian Federation, unique project identifier RFMEFI57717X0239.

CONFLICT OF INTEREST

A.L. Maksimov is the Editor-in-Chief of Zhurnal Prikladnoi Khimii/Russian Journal of Applied Chemistry; the other coauthors declare that they have no conflict of interest.

REFERENCES

1. Talmadge, M.S., Baldwin, R.M., Biddy, M.J., McCormick, R.L., Beckham, G.T., Ferguson, G.A., Czernik, S., Magrini-Bair, K.A., Foust, T.D., Metelsk, P.D., Hetrick, C., and Nimlos, M.R., *Green Chem*., 2014, vol. 16, pp. 407–453.
2. Mortensen, P.M., Grunwaldt, J.-D., Jensen, P.A., Knudsen, K.G., and Jensen, A.D., *Appl. Catal. A: General*, 2011, vol. 407, nos. 1–2, pp. 1–19.
3. Wildschut, J., Mahfud, F.H., Venderbosch, R.H., and Heeres, H.J., *Ind. Eng. Chem. Res*., 2009, vol. 48, pp. 10324–10334.
4. Zhang, X., Zhang, Q., Wang, T., Ma, T., Yu, Y., and Chen, L., *Bioresource Technol*., 2013, vol. 134, pp. 73–80.
5. Chen, C.-J., Lee, W.-S., and Bhan, A., *Appl. Catal. A: General*, 2016, vol. 510, pp. 42–48.
6. Echeandia, S., Arias, P.L., Barrio, V.L., Pawelec, B., and Fierro, J.L.G., *Appl. Catal. B: Environmental*, 2010, vol. 101, pp. 1–12.
7. Olcese, R., Bettahar, M.M., Malaman, B., Ghanbaja, J., Tibavizco, L., Petitjean, D., and Dufour, A., *Appl. Catal. B: Environmental*, 2013, vol. 129, pp. 528–538.
8. Sun, J., Karim, A.M., Zhang, H., Kovarik, L., Li, X.S., Hensley, A.J., McEwen, J.-S., and Wang, Y., *J. Catal*., 2013, vol. 306, pp. 47–57.
9. Lee, C.R., Yoon, J.S., Suh, Y.W., Choi, J.W., Ha, J.M., Suh, D.J., and Park, Y.K., *Catal. Commun.,* 2012, vol. 17, pp. 54–58.
10. Gutierrez, A., Kaila, R.K., Honkela, M.L., Slioor, R., and Krause, A.O.I., *Catal. Today*, 2009, vol. 147, pp. 239–246.
11. Maximov, A.L., Zolotukhina, A.V., Kulikov, L.A., Kardasheva, Y.S., and Karakhanov, E.A., *React. Kinet*., *Mech. Catal.*, 2016, vol. 117, no. 2, pp. 729–743.
12. Maximov, A.L., Zolotukhina, A.V., Mamedli, A.A., Kulikov, L.A., and Karakhanov, E.A., *ChemCatChem.,* 2018, vol. 10, no. 1, pp. 222–233.
13. Vinokurov, V.A., Glotov, A.P., Chudakov, Y.A., Stavitskaya, A.V., Ivanov, E.V., Gushchin, P.A., Zolotukhina, A.V., Maximov, A.L., Karakhanov, E.A., and Lvov, Yu.M., *Ind. Eng. Chem. Res.,* 2017, vol. 56,

no. 47, pp. 14043–14052.

14. Karakhanov, E.A., Maximov, A.L., Zolotukhina, A.V., Mamadli, A.A., Vutolkina, A.V., and Ivanov, A.O., *Catalysts*, 2017, vol. 7, no. 3, pp. 86–112.
15. Venderbosch, R.H., Ardiyanti, A.R., Wildschut, J., Oasmaa, A., and Heeres, H.J., *J. Chem. Technol. Biotechnol*., 2010, vol. 85, pp. 674–686.
16. Yao, G., Wu, G., Dai, W., Guan, N., and Li, L., *Fuel*, 2015, vol. 150, pp. 175–183.
17. Yang, Y., Ochoa-Hernández, C., de la Peña O'Shea, V.A., Pizarro, P., Coronado, J.M., and Serrano, D.P., *Appl. Catal. B: Environmental*, 2013, vol. 145, pp. 91–100.
18. Kniazeva, M.I. and Maximov, A.L., *Catalysts,* 2018, vol. 8, no. 12, p. 644.
19. Bykova, M.V., Bulavchenko, O.A., Ermakov, D.Y., Lebedev, M.Y., Yakovlev, V.A., and Parmon, V.N., *Catal. Ind.*, 2011, vol. 3, pp. 15–22.
20. Vutolkina, A.V., Glotov, A.P., Zanina, A.V., Mahmutov, D.F., Maximov, A.L., Egazar'yants, S.V., and Karakhanov, E.A., *Catal. Today*, 2019, vol. 329, pp. 156–166.
21. Glotov, A., Stavitskaya, A., Chudakov, Y., Ivanov, E., Huang, W., Vinokurov, V., Zolotukhina, A., Maximov, A., Karakhanov, E., and Lvov, Y., *Bull. Chem. Soc. Jpn*., 2019, vol. 92, no. 1, pp. 61–69.
22. Naranov, E.R. and Maximov, A.L., *Catal. Today*, 2019, vol. 329, pp. 94–101.
23. Phan, T.N. and Ko, C.H., *Catal. Today*, 2018, vol. 303, pp. 219–226.
24. Velu, S., Kapoor, M.P., Inagaki, S., and Suzuki, K., *Appl. Catal. A: General*, 2003, vol. 245, pp. 317–331.
25. Wang, Y., Wu, J., and Wang, S., *RSC Adv*., 2013, vol. 3, pp. 12635–12640.
26. Glotov, A., Levshakov, N., Stavitskaya, A., Artemova, M., Gushchin, P., Ivanov, E., Vinokurov, V., and Lvov, Y., *Chem. Commun.,* 2019, vol. 55, pp. 5507–5510.
27. Glotov, A., Levshakov, N., Vutolkina, A., Lysenko, S., Karakhanov, E., and Vinokurov, V., *Catal. Today*, 2019, vol. 329, pp. 135–141.
28. Wang, L., Zhang, J., Yi, X., Zheng, A., Deng, F., Chen, Ch., Ji, Y., Liu, F., Meng, X., and Xiao, F.-Sh., *ACS Catal*., 2015, vol. 5, no. 5, pp. 2727–2734.
29. Hunns, J.A., Arroyo, M., Lee, A.F., Escola, J.M., Serrano, D., and Wilson, K., *Catal. Sci. Technol*., 2016, vol. 6, pp. 2560–2564.
30. Naranov, E.R., Sadovnikov, A.A., Maximov, A.L., and Karakhanov, E.A., *Micropor. Mesopor. Mater*., 2018, vol. 263, pp. 150–157.
31. Naranov, E.R., Badeeva, A.S., Sadovnikov, A.A., Kardashev, S.V., Maksimov, A.L., Lysenko, S.V., Vinokurov, V.A., and Karakhanov, E.A., *Petrol. Chem*., 2016, vol. 56, no. 7, pp. 599–606.
32. Roldugina, E.A., Naranov, E.R., Maximov, A.L., and Karakhanov, E.A., *Appl. Catal. A: General*, 2018, vol. 553C, pp. 24–35.
33. Serrano, D.P., Escola, J.M., Briones, L., Medina, S., and Martínez, A., *Fuel*, 2015, vol. 144, pp. 287–294.
34. Glotov, A.P., Stavitskaya, A.V., Chudakov, Ya.A., Artemova, M.I., Smirnova, E.M., Demikhova, N.R., Shabalina, T.N., Gureev, A.A., and Vinokurov, V.A., *Petrol. Chem*., 2018, vol. 58, no. 14, pp. 1221–1226.
35. Pavankumar, V., Srikanth, Ch.S., Rao, A.N., and Chary, K.V.R., *J. Nanosci. Nanotechnol*., 2014, vol. 14, no. 4, pp. 3137–3146.
36. Morgan, D.J., *Surf. Interface Anal*., 2015, vol. 47, no. 11, pp. 1072–1079.
37. Xing, J., Song, L., Zhang, C., Zhou, M., Yue, L., and Li, X., *Catal. Today*, 2015, vol. 258, pp. 90–95.
38. Bykova, M.V., Zavarukhin, S.G., Trusov, L.I., and Yakovlev, V.A., *Kinet. Catal*., 2013, vol. 54, no. 1, pp. 40–48.
39. Chiu, Ch., Genest, A., Borgna, A., and Rösch, N., *ACS Catal*., 2014, vol. 4, pp. 4178–4188.